GRANULAR FLOW THROUGH AN ORIFICE: SOLVING THE FREE FALL ARCH PARADOX

S.M. Rubio-Largo[1], A. Janda[2], I. Zuriguel[1], D. Maza[1] and R.C. Hidalgo[1],

[1] Department of Physics and Applied Mathematics. University of Navarra. Navarra. Spain.
[2] School of Engineering. University of Edinburgh. Edinburgh. United Kingdom.

Key words: Granular Materials, DEM, Particle Flow

Abstract. Several theoretical predictions of the mass flow rate of granular flows through outlets are based on the existence of a *free fall arch* region covering the silo outlet. Early in the nineteenth century, it was suggested that the particles crossing this region lose their kinetic energy and start to fall freely under their own weight. However, there is not conclusive evidence of this hypothetical region. We examined experimentally and numerically the micro-mechanical details of the particle flow through an orifice placed at the bottom of a silo. Remarkably, the contact stress monotonously decreases when the particles approach to the exit and it only vanishes just at the outlet. The behavior of this magnitude was practically independent of the size of orifice indicating that particle deformation, is insensible to the size of the aperture. Contrary, the behavior of the kinetic stress puts on evidence that the outlet size controls the propagation of the velocity fluctuations inside the silo. Examining this magnitude, we conclusively argue that indeed there is a well-defined transition region where the particle flow changes its nature. Above this region, the particle motion is completely correlated with the macroscopic flow. Our outcomes clarifies why the *free fall arch* picture has served as an approximation to describe the flow rate in the discharge of silos.
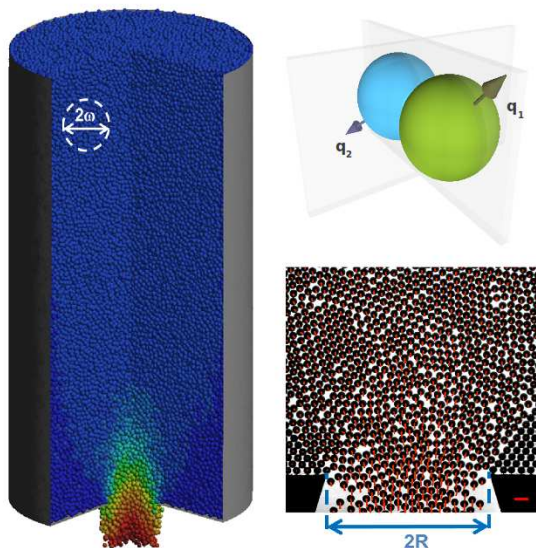
Figure 1: (a) Numerical three-dimensional silo, the color of the particles indicates the velocity in the vertical direction. (b) Sketch of the numerical interaction among two colliding particles. (c) A picture of the two-dimensional silo used in the experiments. The red arrows represent the velocity of each grain. The arrow at right bottom is equivalent to $500mm/s$.

1 INTRODUCTION

Predicting the mass flow rate during silo discharging has been thoroughly attempted in the past years [1, 2, 3]. In general, theoretical frameworks rest on the existence of region close to the orifice where the inter-particle forces diminish and, below this vault, fall due to gravity. Long time ago, this was postulated by Brown & Richards [2], who introduced the concept of *free-fall arch*. Nowadays, this conception is fully accepted and researchers commonly relate it with Beverloo' correlation [4]. However, the *free-fall arch* idea implies the strong formal inconsistency of a spatial stress discontinuity, which is difficult to justify. In addition, recent experimental efforts aimed on proving the existence of such a transition have provided inconclusive outcomes [5, 6].

When examining granular flows experimentally, there are several technical restrictions [7, 8, 9]. Hence, to capture the behavior of three dimensional flows and packings is generally not feasible. In this framework, there is a real need of performing numerical simulations. Discrete element modeling (DEM) is widely accepted as an effective method to address engineering problems concerning dense granular media [10]. Moreover, in applications the formulation of granular macroscopic fields is also necessary. The micro-mechanical details provided by DEM, *i.e.* velocity, position and contacts of individual particles, allow to determine the continuum field profiles, implementing coarse grained average techniques. In this work, we apply a post-processing methodology introduced by I. Goldhirsch [11] and generalized by Weinhart et al [12, 13]. We analyze the granular

flow through an orifice, thoroughly describing the kinetic and dynamic fields.

The paper is organized as follows: in Sec. 2, we describe the experimental setup, the numerical simulations and the theoretical framework of the coarse-grained formulation [11]. Then, in Sec. 3 we explain the implementation of the coarse-grained methodology, which has been used to process both numerical and experimental data, allowing to clarify the nature of the granular flow close to the orifice.

2 METHOD

2.1 Experimental Setup

The experimental setup consists of a quasi-bidimensional silo built with two glass sheets (height $800mm$ and width $200mm$) separated by a steel frame which also conforms the lateral walls (see Fig. 1). The gap between the glass sheets is slightly larger than the particles diameter ($d = 2r_p = 1.0mm$) so the beads can only arrange themselves in a single layer. The particles flow out through a horizontal slit of a tunable aperture $D = 2R$ located at the flat bottom of the silo. The discharge process is recorded by a hight speed camera. The videos were analyzed using image processing techniques allowing a precise determination of the instantaneous position $\vec{r}$ and velocity $\vec{v}$ of each particle. A more detailed description of the experimental setup and image analysis techniques can be found in [14] and [9], respectively.

2.2 Numerical Simulations

In order to model a 3D silo, we have developed a hybrid CPU-GPU Discrete Element [15, 16] algorithm for a system of spheres with $r_p = 1/64\ m$. Initially, we generate a granular column from a granular gas of particles, where particles are located at random positions, within a cylindrical container with flat bottom. Then they settle under the effect of gravity and are allowed to leave the system through a circular outlet, which is located at the bottom of the column. A snapshot of the silo of the numerical three-dimensional silo is shown in Fig. 1.

In the model, each particle ($i = 1...N$) has three translational degrees of freedom and a quaternion formalism has been implemented for describing the 3D angular rotations. The interaction between particle i and particle j is decomposed in normal and tangential directions (see Fig.1). In our approach, the normal interaction is defined by a linear contact and dissipation is introduced using a velocity dependent viscous damping. Our model has been used to simulate spheres with density $\rho = 7520\ kg/m^3$, restitution coefficient $e_n = 0.5$ and $\Delta t = 10^{-6}\ s$. More details about the numerical implementation can be found in [16, 17].

2.3 Coarse Graining Formulation

In order to explore the macromechanical properties of particle flow, a novel coarse graining methodology is used [11, 12]. In both cases, simulations and experiments, we

have accessed to the position and velocities of the particles. According to [11, 12], the microscopic mass density of a granular flow, $\rho(\vec{r})$, at time t is defined as,

$$\rho(\vec{r}) = \sum_{i=1}^{N} m_i \phi(\vec{r} - \vec{r}_i(t)) \tag{1}$$

where the sum runs over all the particles within the system and $\phi(\vec{r} - \vec{r}_i(t))$ is an integrable coarse-graining function. In the same way, the coarse grained momentum density field $P(\vec{r}, t)$ reads as,

$$P(\vec{r}, t) = \sum_{i=1}^{N} m_i \vec{v}_i \phi(\vec{r} - \vec{r}_i(t)) \tag{2}$$

where the $\vec{v}_i$ represent the velocity of particle i. The macroscopic velocity field $\vec{V}(\vec{r}, t)$ is then obtained as the ratio of momentum and density fields,

$$V(\vec{r}, t) = P(\vec{r}, t)/\rho(\vec{r}, t). \tag{3}$$

To calculate the macroscopic stress tensor we have used a mathematically consistent definition of the mean stress tensor $\sigma_{\alpha\beta}$ [11]. Following this approach the total stress field $\sigma_{\alpha\beta}$ can be decomposed by kinetic stress field $\sigma^k{}_{\alpha\beta}$ and contact stress field $\sigma^c{}_{\alpha\beta}$. The mean contact stress tensor reads as,

$$\sigma^c_{\alpha\beta} = -\frac{1}{2} \sum_{i=1}^{N} \sum_{j=1}^{Nc_i} f_{ij\alpha} r_{ij\beta} \int_0^1 \phi(\vec{r} - \vec{r}_i + s\vec{r}_{ij}) ds \tag{4}$$

where the sum runs over all the contacting particles i, j, whose center of mass are at $\vec{r}_i$ and $\vec{r}_j$, respectively. Moreover, $\vec{f}_{ij}$ accounts for the force exerted by particle j on particle i and $\vec{r}_{ij} \equiv \vec{r}_i - \vec{r}_j$.

The kinetic stress field reads as,

$$\sigma^k_{\alpha\beta} = -\sum_{i}^{N} m_i v'_{i\alpha} v'_{i\beta} \phi(\vec{r} - \vec{r}_i(t)), \tag{5}$$

where $\vec{v}'_i$ accounts for the velocity fluctuation of particle i, respect to the mean field.

$$\vec{v}'_i(t, \vec{r}) = \vec{v}_i(t) - \vec{V}(\vec{r}, t). \tag{6}$$

Based on the previous theoretical framework, we have implemented a post-processing tool, which has allowed us to examine the $2D$ and $3D$ kinetic and dynamic fields obtained experimentally and numerically.
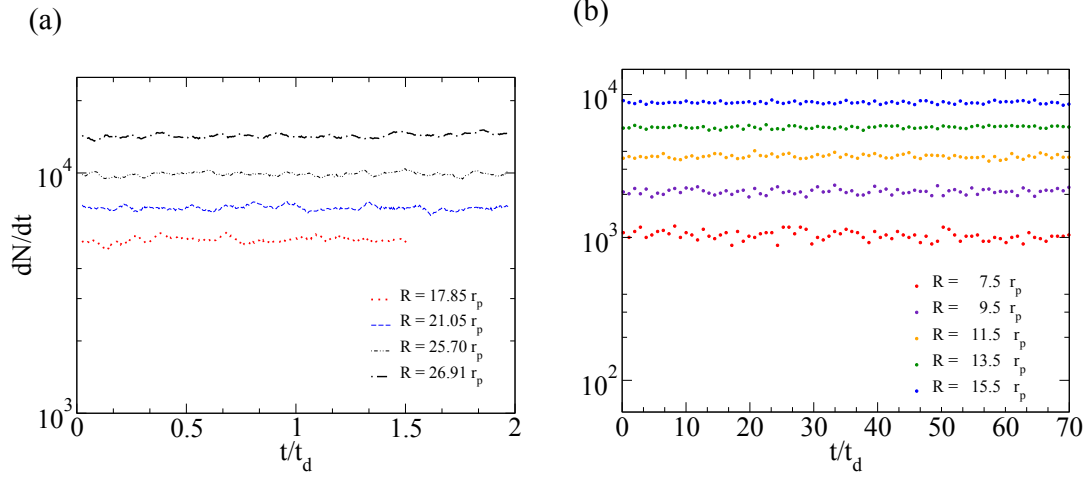
(a)

(b)

Figure 2: The time evolution of the flow rates in terms of the characteristic time $t_d = \sqrt{\frac{2r_p}{g}}$ are shown for different outlet sizes. In a) experimental and b) simulations

3   RESULTS AND DISCUSSION

Our aim is to determine the micro-mechanical properties of a granular flow during a silo discharge. Thus, the complexity of the particle flow was explored experimentally and numerically in a region close to the silo aperture. Additionally, the simulations give the micromechanical details and the contact forces of all particles within the silo.

First, we have determined the particle' flow rate through the surface of the outlet. Experimental and numerical outcomes are exposed for several apertures in Fig.2.3a and Fig.2.3b, respectively. The time evolution of the flow rate dN/dt in particles per second is shown in terms of the characteristic time scale $t_d = \sqrt{\frac{2r_p}{g}}$,*i.e.* the time elapse in which a particle moves its own diameter. In all cases, it is noticeable the system quickly evolves to a steady state characterized by a constant flow rate. This fact allows us to use the coarse-graining methodology, describing the micro-mechanical details of the particle flow [11, 12, 18].

As a second step, we have thoroughly examined the outcomes of the coarse-graining methodology described in Sec. 2.3. To this end, two different coarse-graining functions $\phi(\vec{r})$ have been studied. It is know that $\phi(\vec{r})$ should be an integrable normalized function. First, we have implemented the method with a Heaviside function

$$\phi_h(\vec{r}) = \frac{1}{\Omega_d(\omega)} H(\omega - |\vec{r}|).\tag{7}$$

and as second choice, we have used a Gaussian

$$\phi_g(\vec{r}) = \frac{1}{(\sqrt{2\pi}w)^3} \exp\left(-\frac{|\vec{r}|^2}{2w^2}\right).\tag{8}$$

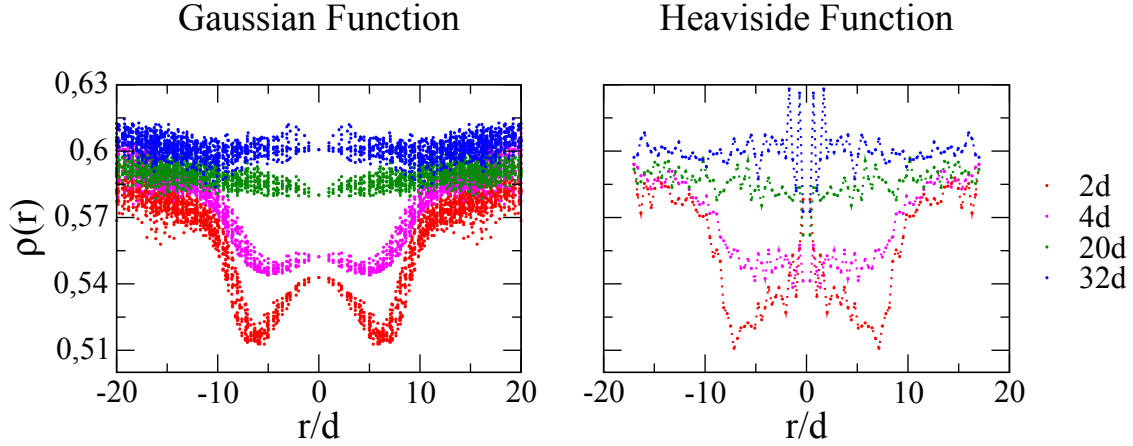## Gaussian Function   Heaviside Function

Figure 3: Mass density profiles of a granular flow, $\rho(\vec{r})$, using Gaussian (left) and (right) Heaviside coarse-graining functions. The measurement has been obtained at different heights from the base of the silo. The orifice size of the silo is $R = 16d$ and the coarse graining scale $w = d$.

In Fig.3, the mass density profiles $\rho(\vec{r})$ of a $3D$ numerical granular flow are shown. Outcomes obtained using two different integrable functions Heaviside Eq. 7 and Gaussian Eq. 8 are illustrated . Note, the measures were done at different heights respect to the silo outlet, covering from $z = 2d$ to $z = 32d$ where d is the particle diameter. As can be observed, both coarse-graining functions give equivalent outcomes for the density profiles. However, the Gaussian function produces smoother results for the same coarse graining scale $w = d$. In the following, the data processing has been done using the Gaussian function $\phi(\vec{r}) = \phi_g(\vec{r})$. At the end of this work, we will clarify the role of the coarse-graining scale w.

Given the positions and velocities of all particles, one can fully describe the steady state kinetic fields in the whole silo. In Fig. 4 we plot the average velocity fields obtained numerically in a $3D$ silo with an orifice of $R = 16d$. The profiles of the radial velocity $v_r(r)$ at different heights are shown in Fig. 4(right). As it can be expected, the radial absolute velocity field diminishes at the center of the silo, that is clearly explained by symmetry reasons. Note, that the magnitude $v_r(r)$ is comparable with the magnitude of $v_z(r)$ and the location of the maximum absolute radial velocity $\mid v_r(r) \mid$ only slightly changes with the height from the orifice. Additionally, in Fig. 4(left), the vertical velocity fields $v_z(r)$ are also illustrated. The Gaussian shape of the velocity profiles $v_z(r)$ is in excellent agreement with those experimentally obtained [19]. Moreover, in the past it has been proven that this behavior is compatible with the solution of a diffusive-like equation [20]

Additional macromechanical details of the particle flow can be extracted studying the changes in the stress field. In Fig.5a, we plot the spatial behavior of the *contact pressure*,
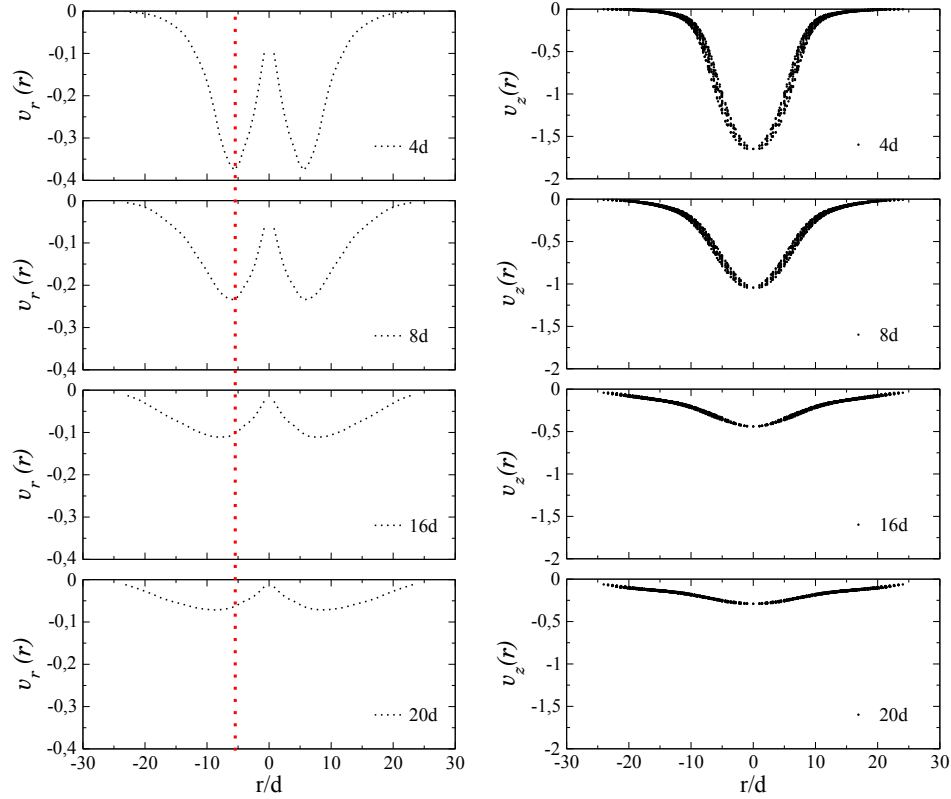
Figure 4: On the left, radial component of the velocity at different heights from the orifice (velocity measured in units of diameter of particle per second). On the right, vertical component of the velocity at different heights from the orifice. The measurements have been done for the simulation of a 3D silo with an orifice size of $R = 16d$ (heights of $z = 4d$, $z = 8d$, $z = 16d$ and $z = 20d$, respectively). In all cases, the units are diameter/sec.

which was estimated using trace and the deviatoric of the contact stress field σ^c. Note that the *contact pressure* results in a monotonous decreasing function that correlates with the increase of the dilatancy, which achieves a maximum at the outlet [9, 17]. Here, it is important to remark that the values of *contact pressure* were nearly independent on the outlet size [18]. Accordingly, a region resembling a *free-fall arch* (that should scale with R) can not be inferred from these findings.

Complementary, we have anylized the strength of the *kinetic pressure* field calculating the trace and the deviatoric of the mean kinetic stress tensor σ^k, defined by Eq.(5) (see Fig. 5b). Although the strength of the *kinetic pressure* results several order of magnitude smaller than the *contact pressure*, its spatial pattern reveled novel micro-mechanical details. The *kinetic pressure* field evidenced conclusively the existence of a well defined transition region. Both, experimental and numerical outcomes suggest that above a well
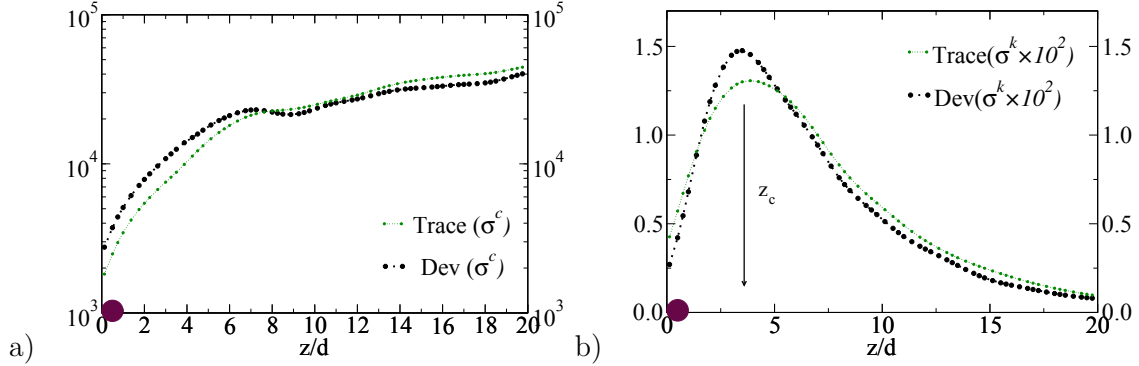
Figure 5: Trace and deviator of the a) contact stress mean field tensor $\sigma_{\alpha\beta}^c$ and b) kinetic stress mean field tensor, $\sigma_{\alpha\beta}^k$.

defined surface the particles follow the global macroscopic laminar flow [18]. The latter correlates with the diminishing of the *kinetic pressure* with the height and indicates the mass transport within the silo is mainly advective. However, as the particles get closer to the orifice their individual movement decorrelates respect to the global flow and, accordingly, the *kinetic pressure* shows a maximum value at the transition surface $z_c(r)$. After crossing, the particles start to fall by gravity and the contacting stress gradient slowly diminishes as one gets closer to the outlet.

In Fig.6, we present the universal surface z_c/R that characterizes the transition region. We illustrate outcomes corresponding to two different orifices obtained experimentally. Remarkably, we have found the transition surface is independent of the outlet size. For testing the consistency of our results, the post-processed experimental data was analyzed using different coarse-graining scales. As it noticeable the findings are totally compatible within our experimental errors. The data collapse clearly proves the existence of a parabolic transition arch. For comparison, two truncate paraboloids $\alpha\left(1-(r/R)^2\right)$ have been included in the graph.

Astonishing, all the curves z_c/R obtained for different outlet sizes can be collapsed [18]. Moreover, we have found excellent qualitative agreement in wide domain of apertures for both experimental and numerical outcomes [18]. Hence, we have identified a region where the collisional part of the stress tensor starts to diminish and the dynamics becomes gradually dominated by the external field. The scaling of this surface with the size of the aperture links the observed dynamics in the discharge process with the stress fields inside the silo. This picture contrasts with the traditional view of the existence of a *free fall arch* region where the velocity is negligible and grains start a free fall.
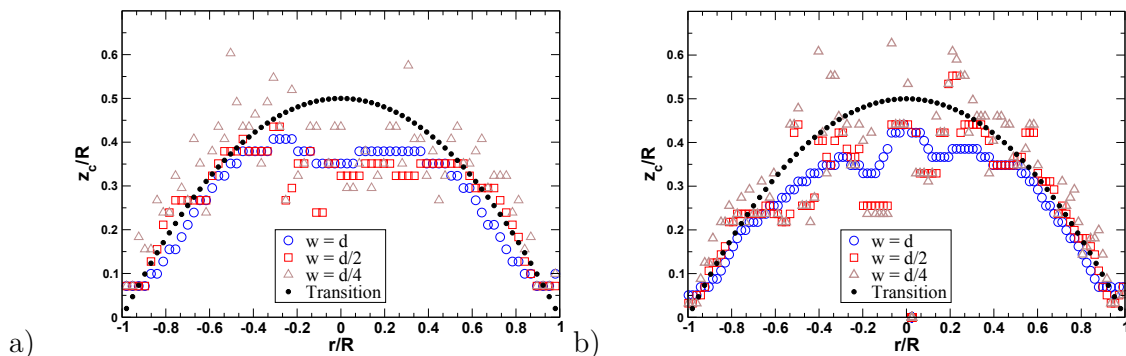
Acknowledgements

Figure 6: Position of the local maximum z_c/R of the *kinetic pressure* as a function of the radial distance. Experimental results are illustrated for (a) $R = 17d$ and (b) $R = 26d$. Testing the consistency, several values of the coarse-graning scale w has been used. For comparison, truncate paraboloids $\alpha \left(1 - (r/R)^2\right)$ have also shown.

for a scholarship.

REFERENCES

[1] B.P Tighe and M. Sperl, *Granular Matter*, **9**, 141–144 (2007).

[2] R. C. Brown and J. C. Richards, *Principles of Powder Mechanics,* Pergamon Press, 1970.

[3] R. M. Nedderman, *Statistics and kinematics of granular materials,* Cambridge University Press, 1992.

[4] W. A. Beverloo, H. A. Leniger, and J. J. Van de Velde, *Chem. Eng. Sci.* **15**, 260 (1961).

[5] F. Vivanco, Sergio Rica and F. Melo, *Granular Matter* **14**, 563 (2012).

[6] D.J. Van Zuilichem, N.D. Van Egmond, and J.G. De Swart, *Powder Technology* **10**, 161 (1974).

[7] C. Mankoc, A. Janda, R. Arévalo, J. M. Pastor, I. Zuriguel, A. Garcimartn and D. Maza *Granular Matter* **9** 407 (2007).

[8] I. Zuriguel, A. Garcimartín, D. Maza, L.A. Pugnaloni and J.M. Pastor. *Phys. Rev. E* **71** 051303 (2005)

[9] A. Janda, I.Zuriguel, and D.Maza, *Phys. Rev. Lett.* **108**, 248001(2012).

[10] T. Pöschel, T. Schwager, Computational Granular Dynamics, Springer-Verlag Berlin Heidelberg New York, 2005.

[11] I. Goldhirsch, *Granular Matter* **12**, 239 (2010).

[12] T. Weinhart, A. R. Thornton, S. Luding, and O. Bokhove, *Granular Matter* **14**, 531, (2012).

[13] T. Weinhart, R. Hartkamp, A. R. Thornton, and S. Luding, *Phys. Fluids* **25**, 070605, (2013)

[14] A. Janda, I.Zuriguel, I.A.Garcimartn, L.A.Pugnaloni and D.Maza, *Europhys. Lett.* **84**, 44002(2008).

[15] J. Owens, M. Houston, D. Luebke, S. Green, J. Stone, and J. Phillips, *Proceedings of the IEEE* **96**, 879-899 (2008).

[16] R. C. Hidalgo, T. Kanzaqui, T. Alonso-Marroquin and S. Luding *AIP Conf.Proc.* **1542**, 169-172 (2013).

[17] D. Maza, A. Janda, S.M. Rubio-Largo, I. Zuriguel and R.C. Hidalgo, *AIP Conf. Proc.* **1542**, 674 (2013).

[18] S.M. Rubio-Largo, A. Janda, I. Zuriguel, D. Maza and R.C. Hidalgo. *Phys. Rev. Lett.* (2015)
http://journals.aps.org/prl/accepted/34076Y19Md515b4914c8754174498186553516e7f

[19] A. Garcimartín, I. Zuriguel, A. Janda and D. Maza. it Phys. Rev. E **84**, (2011), 031309

[20] R. M. Nedderman and U. Tüzün, *Powder Technol.* **22**, 243 (1979)